ADVANCED HEALTHCARE MATERIALS
www.advhealthmat.de

Self-Normalized Detection of ANXA3 from Untreated Urine of Prostate Cancer Patients without Digital Rectal Examination

*Minhong Jeun, Sungwook Park, Yongdeok Kim, Jaewon Choi, Sang Hoon Song, In Gab Jeong, Choung-Soo Kim, and Kwan Hyi Lee**

A noninvasive quantitative assay that is capable of identifying prostate cancer biomarkers in untreated urine is an attractive diagnosis tool, but this method is subject to various obstacles. Difficulties presented by untreated urine include varying salt concentrations, and pH levels that may be different even though they are from the same patient. Untreated urine also presents interference from other biomolecules and possesses a fewer number of cancer biomarkers than can be found in serum. As a result, urine preconditioning processes and digital rectal examination (DRE) to increase biomarker secretion are mandatory in current urine assays. To address these challenges, an ion-responsive urine sensor (IRUS) that measures differential electrical signals is proposed as a self-normalized detection method. The proposed IRUS is based on a FET biosensor with a disposable sensing gate and has the capability to detect the prostate cancer antigen ANXA3 in untreated patient urine. The IRUS can detect ANXA3 at <1 fg mL^{-1} with high reliability. In addition, it is found that ANXA3 levels in urine show clinically significant correlation with real tumor volumes. This paper provides a guideline in developing a clinically ready accurate noninvasive platform, which is capable of predicting prostate cancer using untreated urine without DRE.

1. Introduction

Urine-based assays are a very attractive monitoring system in that the specimen of interest, urine, can be available via noninvasive procedures.[1–4] Urine contains various biomarkers, including urogenital organ based biomarkers from the prostate, bladder, and kidney.[4] These urogenital biomarkers are unique because they are a result of direct contact with the urogenital organs.[4] Therefore, biosensors that can directly detect these urogenital biomarkers in urine are considered to be an ideal noninvasive diagnostic tool for cancers or other diseases in the field of urology.

Among the various urological diseases, prostate cancer is not only the most common cancer, but it is one of the leading causes of cancer-related death among the Caucasian males in both the United States and Europe.[5,6] Contemporary diagnostic methods of prostate cancer such as digital rectal examination (DRE), prostate surface antigen (PSA) screening, and transrectal ultrasound (TRUS)-guided biopsy are invasive and inaccurate due to various reasons such as the low specificity of PSA, subjectivity of DRE, and side effects during TRUS.[7,8] In this regard, a biosensor that can directly detect biomarkers of prostate cancer in urine can be a powerful noninvasive diagnostic tool that is patient friendly, simple, and fast.

Choosing an optimal biomarker from urine samples which has high prostate cancer specificity is also important for prostate cancer diagnosis. Currently prostate-specific antigens (PSA) are used as the gold standard during initial screening of prostate cancer,[9–11] but the frequency of false positive and false negative from PSA assays have coerced researchers to search for more efficient alternatives.[4] The annexin A3 (ANXA3) has the high specificity (≈90%) and demonstrated to be a promising biomarker for prostate cancer, as can be seen in a clinical study with 591 patients.[12] The expression of ANXA3 in tumor tissue is associated with a Gleason score and the T stage, while there is little correlation between PSA level in serum and the tumor state.[13]

Sample in urines presents many challenges during clinical urine analyses. The condition of urine depends on the patient to a great degree. The urine condition changes on the time of day, and on the hydration status of the patient, and these conditions are especially inconsistent to urine sample procured without the invasive DRE process. Varying conditions in untreated urine include salt concentration and pH levels that

Dr. M. Jeun, S. Park, Y. Kim, J. Choi, Prof. Dr. K. H. Lee
Center for Biomaterials
Biomedical Research Institute
Korea Institute of Science and Technology (KIST)
5 Hwarang-ro 14-gil, Seongbuk-gu, Seoul 02792, Republic of Korea
E-mail: kwanhyi@kist.re.kr
S. Park, J. Choi, Dr. K. H. Lee
Department of Biomedical Engineering
Korea University of Science and Technology (UST)
217 Gajeong-ro, Yuseong-gu, Daejeon 34113, Republic of Korea
Prof. Dr. S. H. Song, Prof. Dr. I. G. Jeong, Prof. Dr. C.-S. Kim
Department of Urology
Asan Medical Center
University of Ulsan College of Medicine
88 Olympic-ro 43-gil, Songpa-gu, Seoul 05505, Republic of Korea
The ORCID identification number(s) for the author(s) of this article can be found under https://doi.org/10.1002/adhm.201700449.

DOI: 10.1002/adhm.201700449

fluctuate depending on the patient, which in turn greatly affect the sensing performance. Even urine samples from a same person can be different according to his or her physiological condition. Such sample variation makes it difficult for a urine assay to properly measure a biomarker. For these reasons, existing urine sensor platforms have relatively low sensitivity and require urine pretreatment process.[12,14–16] Aside from this, DRE is indispensably required to increase the secretion of biomarkers due to a trace number of biomarkers existing in a bare urine without DRE.[15,17] For these reasons, the quantification of ANXA3 in a patient urine was difficult using the existing platforms and the pretreatment and DRE had to be preceded for their measurement systems.[12,18] Even though the DRE is a very effective way to increase the quantity of biomarkers in urine, DRE is an invasive method, which is dependent on the experience of the examiner.

In this research, we proposed a self-normalized urine assay using FET-based ion-responsive urine sensor (IRUS) with a disposable sensing gate. The proposed IRUS successfully measured and quantified ANXA3 in untreated patient urine without DRE. To minimize the different conditions that are different for each different urine sample, a self-normalized detection method was proposed by measuring reference signals from each patient's urine sample (**Figure 1**). Calibration of the detected signal with the differential signal enabled the accurate analysis of ANXA3 regardless of various urine conditions. The disposable sensing gate plays a role in improving the stability of the IRUS by preventing contamination from urine by separating the sensing portion of the sensor from the transistor portion of the sensor. The precisely designed dual-gate structure was used to enhance sensitivity in the measurement of ANXA3 from untreated urine by improving the capacitive coupling between the top and bottom gate dielectrics in the thin-film transistor.[19] In addition, we found that the level of ANXA3 in urine has a strong correlation to the real tumor volume of patients. This result is meaningful because tumor volume has a strong relationship with the cancer progression.[20]

2. Results and Discussion

2.1. Measurement of ANXA3 in Patient Urines Using IRUS

We measured the IRUS's electrical properties to evaluate and demonstrate its functionality and performance to be used as a transistor biosensor. The IRUS showed comparable performances with those of our tailored-FET that was reported previously.[19] **Figure 2**a shows transfer curves of the IRUS measured at a back gate sweep mode (BG) and a top gate sweep mode (TG, inset). The IRUS shows well-controlled FET's electrical characteristics including a high on/off ratio (TG: 10^6 and BG: 10^8), a low threshold voltage (TG: –0.37 V and BG: –6.02 V), and a good subthreshold swing (TG: 77 mV dec^{-1} and BG: 1817 mV dec^{-1}) in the both sweep modes. We also investigated the pH sensitivity of the IRUS in both dual-gate and single-gate operation modes, respectively. Figure 2b shows the I_D–V_G curves of dual-gate and single-gate IRUS measured in pH 4 and pH 10 buffer solutions. As can be seen in the results, the single-gate mode IRUS showed the typical pH sensitivity value of 56.65 mV pH^{-1}. This value is similar to the Nernst limit (59.6 mV pH^{-1}). In the case of the dual-gate mode, the IRUS showed the highly improved pH sensitivity of 1897 mV pH^{-1}. From these results, we confirmed that the IRUS fabricated by the 6 in. mass production process will be well operated as a biosensor.

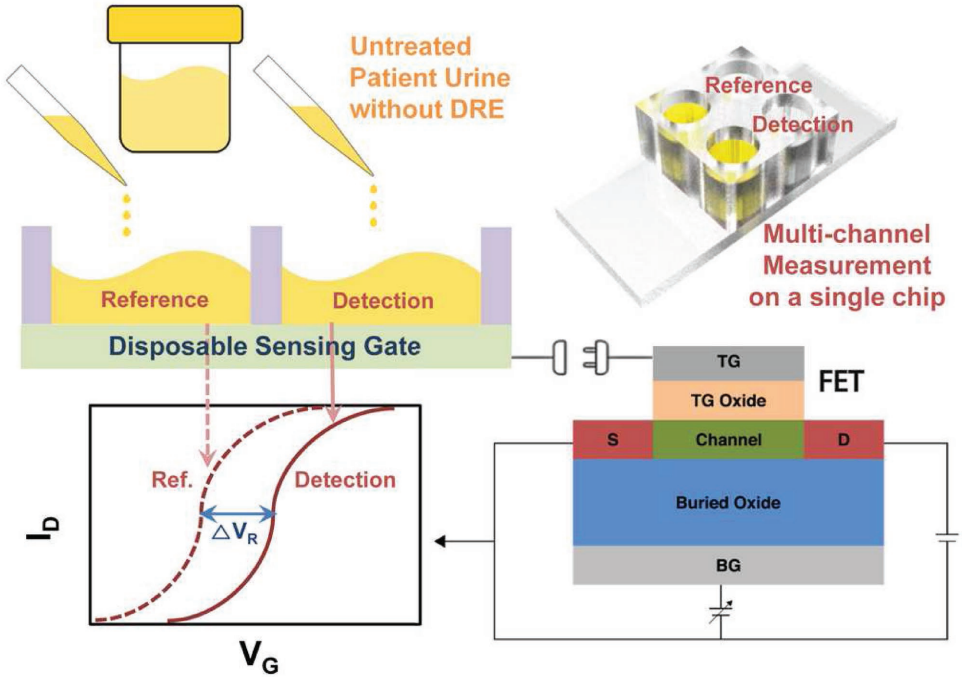

Figure 1. The schematic of the measurement steps for the quantification of a prostate cancer biomarker on a single chip using IRUS from an untreated patient urine sample.

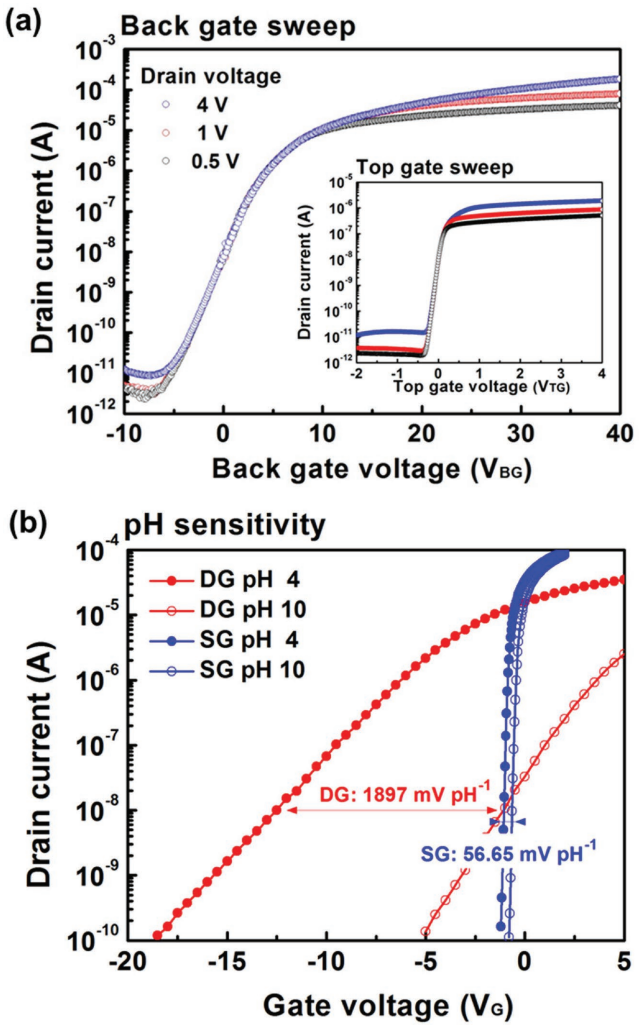

Figure 2. a) Transfer curves of IRUS measured under back gate sweep and (inset) top gate sweep modes, and b) pH sensitivity of dual-gate and single-gate IRUS measured in pH 4 and pH 10 buffer solutions.

In addition to the high sensitivity, the biosensor should have good stability in a urine environment to successfully detect a trace amount of biomarkers existing in urine. In order to evaluate the stability of IRUS in a urine environment, the real-time hysteresis and drift characteristics of the voltage signal between human urine and pH 10 buffer solution were investigated (**Figure 3**a). The inset of Figure 3a shows the disposable sensing gate, which contains the pH 10 buffer solution and urine sample. As can be seen in the result, IRUS showed the highly reliable response characteristics as well as good stability with below 1.75% error range for 60 min. Considering that the measurement process for detecting biomarkers in patient urine takes about 20 min, this result strongly supports that IRUS can stably measure the biomarkers in patient urine. Furthermore, the disposable sensing gate not only prevents the transducer of IRUS from being contaminated by the various ions in the urine but also improves the usability of IRUS in its application as a urine assay.

Prior to detecting ANXA3 in patient urine, a standard curve for ANXA3 was acquired using the artificial urine spiked ANXA3 from 0.1 fg mL^{-1} to 10 µg mL^{-1}. The standard curve provides the sensing performances of IRUS such as sensitivity, linearity, detectable (or dynamic) range, and limit of detection (LOD) as well as giving us data for quantitative analysis of biomarkers. Figure 3b shows the I_D–V_{BG} results regarding various ANXA3 concentration measure with the anti-ANXA3 immobilized disposable sensing gate. It shows the linear region of I_D–V_G curves according to ANXA3 concentrations. The full graphs were measured under applied the bottom gate voltage sweeping from –40 to 40 V. As the concentration of ANXA3 increases from 0.1 fg mL^{-1} to 10 µg mL^{-1}, the I_D–V_{BG} curves shift positively caused by the change in surface potential by the antigen–antibody reaction.[21,22]

Figure 3c exhibits the standard curve according to the ANXA3 concentration. The IRUS showed a good linearity of 96.15%, a high sensitivity of 33.3 mV dec^{-1}, and a low LOD of less than 1 fg mL^{-1}. As can be seen from the graph, the IRUS becomes saturated around 10^{-6} g mL^{-1}. A slight decrease in voltage shift is experienced around 10^{-5} g mL^{-1}, but this is within the error range of the detection signal. These significant sensing performances compared with those of other urine FET sensors strongly demonstrate that IRUS can be successfully used for the noninvasive detection of prostate cancer's biomarkers in the untreated urine collected without DRE.[16,17] The results demonstrate that the self-normalization method using the disposable sensing gate is well worked to detect ANAX3 in urine with high reliability as well as, the dual-gate structure of IRUS is built to have a high capacitive coupling ratio for improving the sensitivity.[19,23] Additionally, the good linearity to the ANXA3 with a wide detectable (or dynamic) range of 10^{10} implies that the IRUS can quantitatively analyze wide range of biomarker concentrations.

Detection of ANXA3 in untreated patient urine suffers from variable sample conditions such as salt concentrations, pH levels, and other impurities etc.[4] The various conditions greatly affect the ion concentrations in urine. Since the IRUS is very sensitive to small changes in ion concentration, these unwanted sample conditions may negatively affect the sensing electrical signal and cause misdiagnosis. In this study, in order to minimize the effect, we measured an additional I_D–V_{BG} curve (reference signal) in another well which was not coated with the target antibodies. This well had the same urine sample inserted into it. Thus, we had two electrical signals: (1) a detection signal which reflected antigen–antibody reactions, and (2) a reference signal which did not have such reactions. We subtracted the reference signal (the signal obtained from the well that was not coated with antibodies) from the detection signal (the signal obtained from the well that had coated antibodies). This voltage difference (or shift) is the electrical sensing signal depending on the ANXA3 concentration without the effect of the unfavorable conditions, such as reactions with other proteins. As can be seen in Figure 1, the multichamber structure of polydimethylsiloxane (PDMS) in a disposable sensing gate enabled the measurement of two I_D–V_{BG} (detection and reference signals) curves on a single chip.

To quantify the concentration of ANXA3 in patient's urine samples, we prepared 34 patients' urine samples without DRE and pretreatment and detected the ANXA3 using the IRUS. **Figure 4**a shows the representative results of ANXA3 detection

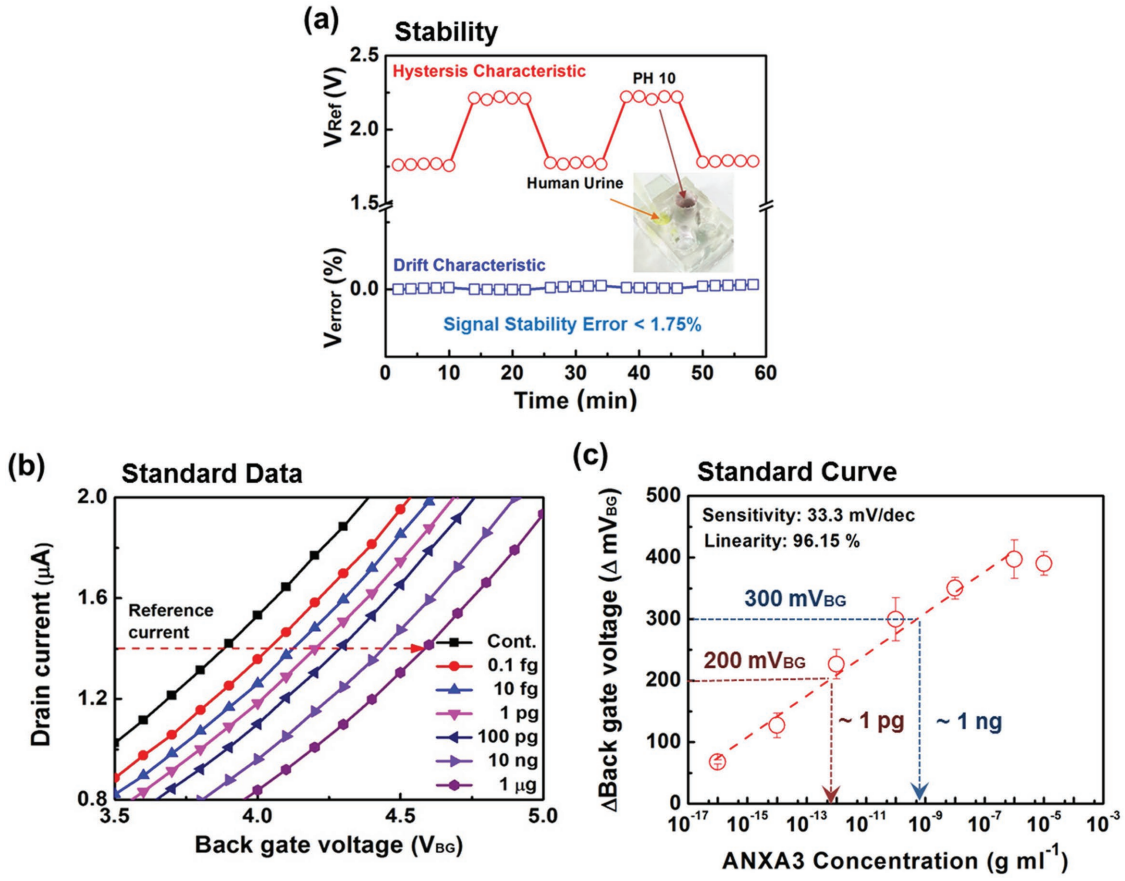

Figure 3. a) The real-time hysteresis and drift characteristics of IRUS measured in human urine pH 10 buffer solution. (inset) The disposable sensing gate containing the 80 μL of human urine and pH 10 buffer solution. b) I_D–V_{BG} results of IRUS according to ANXA3 concentrations measured with the anti-ANXA3 immobilized disposable sensing gate. c) Variation of V_{BG} according to different ANXA3 concentrations in IRUS (standard curve). The detection signal becomes saturated around 10^{-6} g mL^{-1}.

and reference I_D–V_{BG} signals measured in the patient's urine (patient # 16 and # 17). As can be seen in the results, the reference I_D–V_{BG} curves varied due to the different conditions such as salt concentration, pH level, and impurity in a patient's urine. Setting each reference signal from a patient's urine was useful for the quantification of only the ANXA3 reaction without having the unwanted effects of various sample conditions. The inset in Figure 4a shows that the detection and reference signal from a patient's urine could be measured on a single disposable sensing gate.

The back gate voltage shifts (ΔV_{BG}) between the detection and reference signals were 378 and 306 mV for the patient # 16 and # 17, respectively, when the drain current was 1 μA. The quantitative results of the ANXA3 concentration for patient # 16 and # 17 were obtained from the standard curve (Figure 3c). In our measurement, the concentrations of ANXA3 in patient urines were 310 and 2.38 ng mL^{-1} for the patient # 16 and # 17, respectively. Figure 4b shows the ΔV_{BG} values and the ANXA3 concentrations for 34 patient's urine samples. Among all the samples, only six samples were not found in the detectable range (false negative rate: 17.64%) of the IRUS. On the other hand, the IRUS shows the very high true positive rate of 82.36%. These results successfully demonstrated that the IRUS can detect ANXA3 prostate biomarker with higher accuracy in the urine samples that did not undergo DRE.

Table 1 shows the selected ΔV_{BG} values and the corresponding ANXA3 concentrations for nine patient's urine

Table 1. PSA levels in serum, prostate volumes, percent tumor volumes, real tumor volumes, ΔV_{BG}, and ANXA3 levels in urine for the selected prostate cancer patients.

Patient	PSA in serum [ng mL^{-1}]	Prostate volume [cm^3]	% tumor volume	Real tumor volume [cm^3]	ΔV_{BG} [mV]	ANXA3 in urine [ng mL^{-1}]
A	5.4	30	10	3	231	0.013
B	15.9	42.13	10	4.213	274	0.226
C	6.4	41	6	2.46	159	0.0007
D	14.6	53.22	8	4.2576	239	0.02
E	10.2	44.5	60	26.7	310	2.64
F	4.7	47.26	10	4.726	180	0.0002
G	6	22.83	5	1.1415	283	0.366
H	27.87	24.7	75	17.4075	297	0.95
I	5.1	32.38	10	3.238	223	0.0053

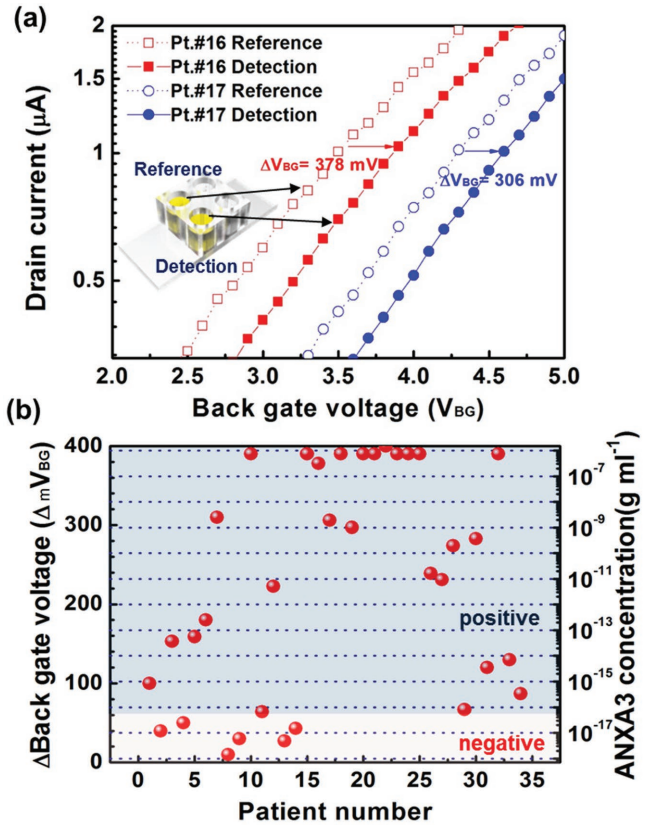

Figure 4. a) I_D–V_{BG} results and ΔV_{BG} between the detection and reference voltages from urine samples of patient # 16 and # 17. b) The results of ΔV_{BG} for all the patient's urine samples and corresponding ANXA3 concentrations calculated from the standard curve. The detectable range (dynamic range) of the IRUS: 10^{-16} –10^{-6} g mL^{-1}.

samples with clinical results. **Table 2** indicates other urine assays for the detection of ANXA3.[12,18,24,25] There have been several reports on detection methods of ANXA3 in urine such as western blot, electrochemical sensing, quartz crystal microbalance, and ELISA. Although quartz microbalance and electrochemical method had a low LOD of less than 100 pg mL^{-1}, they had not been proved clinically. Schostak et al. and Hamelin-Peyron et al. measured ANXA3 in patient's urine. However, DRE had to be preceded in their measurement systems, which means that their sensing systems cannot be considered as a noninvasive method. In this regard, this is the first time a noninvasive method measured the detection of ANXA3 without urine pretreatment and DRE.

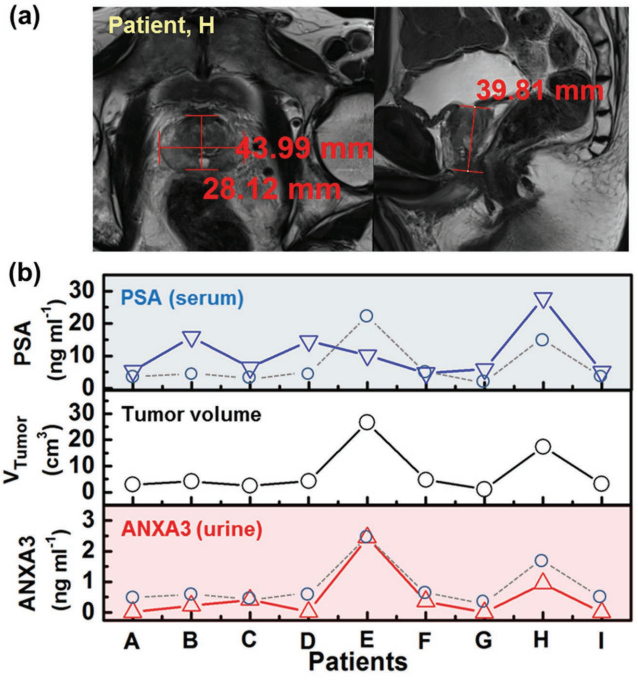

Figure 5. a) Cross sectional and longitudinal MRI images of a prostate cancer. b) PSA levels in serum, real tumor volumes, and ANXA3 levels in urine for the selected prostate cancer patients.

2.2. Clinical Correlation

To validate the clinical correlation between our experimental results and the clinical outcomes of the patients, clinical data including preoperative PSA levels in serum, %tumor volume, prostate volume, and estimated real tumor volume for the patients were analyzed and compared. MRI analyses were conducted to calculate the real tumor volume for patients. **Figure 5**a shows the T2-weighted MRI cross sectional and longitudinal images for the patient E.

In Figure 5a, the transverse diameter, AP diameter, and longitudinal diameter were measured as 43.99, 28.12, and 39.81 mm, respectively, and the prostate volume was calculated to be 24.7 cm^3. Then, the real tumor volume of patient E was calculated as 17.4 cm^3 by multiplication of the calculated prostate volume and %tumor volume. The %tumor volumes for patients were investigated by visual estimation. Table 1 exhibits the preoperative PSA level in serum, %tumor volume, prostate volume, and estimated real tumor volume for the selected nine patients.

Table 2. Urine assays for detection of ANXA3.

Method	Sample	LOD	Pretreatment	DRE	Refs.
Electrochemical	Artificial urine spiked ANXA3	95 pg mL^{-1}	N/A	N/A	[22]
Quartz crystal microbalance	Human urine spiked ANXA3	75 pg mL^{-1}	N/A	N/A	[23]
ELISA	Patient urine	<1 ng mL^{-1}	Yes	Yes	[16]
Western blot	Patient urine	–	Yes	Yes	[10]
IRUS	Patient urine	<1 fg mL^{-1}	No	No	This study

Figure 5b shows the clinical PSA levels measured in serum, real tumor volumes, and ANXA3 levels measured in urine for the nine patients; only nine patients provided consent for both tumor MRI and serum analysis. Since cancer progression is proportional to cancer volume, the volume prediction is an important indicator for diagnosis of prostate cancer and can prevent overtreatment.[20,26] Although PSA level in serum is well known as the golden standard for diagnosis of prostate cancer and reported as a good biomarker associated with tumor volume, the issue has been controversial due to the dependency on the prostate size.[27,28]

The black solid and dotted lines in Figure 5b indicate the real tumor volumes. Comparison between the real tumor volumes and PSA levels in serum shows a similar trend in the curve. However, this pattern is not always matched as can be seen in patient B, E, and G due to the dependency on the prostate volume. On the other hand, in the case of the ANXA3 levels, it was found that there was very small discrepancy in patients C and D. Except for the small discrepancy, the variation trend of the ANXA3 levels were well matched up with the real tumor volumes than those of the PSA levels. This research proposes the possibility of successful prostate cancer diagnosis if miniscule amounts of ANXA3 are able to be sensitively and accurately identified. Additionally, Figure 5b indicates that simultaneous accurate analysis of PSA levels in serum, ANXA3 levels in urine, and prostate volume will lead to a better prediction of tumor volume. These results show the possibility of utilizing multipanel biomarker analysis technology for a more thorough diagnosis of prostate cancer.

3. Conclusion

In this study, we demonstrated a self-normalized detection system by using the IRUS to quantify ANXA3 regardless of the variables in a patient's urine sample. The proposed IRUS was able to measure a trace number of ANXA3 in untreated patient urine even without the need for DRE, a first for its field. The dual-gate and well-defined structure and disposable sensing gate system of IRUS provide high sensitivity, a LOD value of less than 1 fg mL^{-1}, and a stable measurement of untreated urine. In addition, the result of ANXA3 levels in urine showed a clinical correlation with tumor volume. Since cancer progression is usually proportional to cancer volume, the volume prediction can be an important factor for prostate cancer diagnosis. The multipanel analysis with serum PSA levels and urine ANXA3 levels can improve the accuracy for the measurement and prediction of tumor volume. Our study provides a guideline in developing a clinically ready noninvasive platform as well as more accurate tool for prostate cancer diagnosis using untreated urines without DRE.

4. Experimental Section

Fabrication of the IRUS: The IRUS is composed of a dual-gate ion-sensitive FET (ISFET) and a disposable sensing gate. In this study, we set up the mass production protocol for the dual-gate FET by employing the 6 in. wafer semiconductor process and the gate-first fabrication procedure to secure the high reliability in the sensor performances. The ISFET was fabricated using a p-type (100) 6 in. silicon-on-insulator (SOI) wafer to form the dual-gate structure. The thicknesses of the buried oxide (BOX) layer, top silicon layer, and top oxide layer were 750, 100, and 10 nm, respectively. The active region was defined by employing photolithography and etching process using an inductively coupled plasma reactive-ion etching (ICP-RIE) system. The top oxide layer was formed using a dry oxidation method. To form the gate electrode structure, a 150 nm thick TiN was deposited using a sputtering system and the TiN metal layer was etched using photolithography and etching process. The source and drain regions were defined by arsenic (As) ion implantation (concentration: 3×10^{15}). 150 nm thick TiN contact pads on the source and drain were formed by deposition and lift-off processes. A cross-sectional view of the ISFET is displayed in Figure 1 (lower right).

To fabricate the disposable sensing gate, 80 nm thick SnO_2 was deposited on an ITO deposited glass substrate using RF magnetron sputtering system. The RF power was 50 W and the working pressure was 18 mTorr. Then, a PDMS chamber was attached on the SnO_2 layer using an O_2 plasma treatment (upper right of Figure 1). The PDMS chamber is used as a urine reservoir for the antigen–antibody reaction.[29–32] The volume of the reservoir is 80 µL.

Collection and Measurement of ANXA3 in Patient's Urine: The drain current versus back gate voltage (I_D–V_{BG}) curves in IRUS were measured using a high precision semiconductor characterization system (Keithley 4200-SCS)) in a dark box. An Ag/AgCl reference electrode was used as a grounded top reference electrode. To investigate the stability in urine, normal human urine, artificial urine, and a commercial pH 10 buffer solution were used. The artificial urine is composed with 36.4 g of urea, 15.0 g of sodium chloride, 9.0 g of potassium chloride, 9.6 g of sodium phosphate, 4.0 g of creatinine, 100 mg of albumin, and 1.5 L of distilled water.[33] The ANXA3 standard curve was established by calculating the difference between the detection and reference I_D–V_G curves.

For the detection measurement of the ANXA3 standard curve, an 80 µL of artificial urine with ANXA3 was injected onto the anti-ANXA3-immobilized sensing membrane and the reaction was run for 20 min. This result was then compared with the I_D–V_{BG} curve. Then, the previous solution was washed out using a PBS buffer solution and the same procedure was repeated by injecting artificial urine containing the ANXA3 in the order of increasing concentration from 0.1 fg mL^{-1} to 10 µg mL^{-1}.

The reference measurement was obtained by applying the same patient's urine unto a sensing membrane that did not possess and conjugated ANXA3 antibodies. The same detection measurement protocol was utilized. For the measurement of ANXA3 in a patient's urine, the urine samples from 34 patients without DRE were collected from Asan Medical Center. All the urine samples and clinical results were obtained from the patients after informed consent according to the guidelines of Asan Medical Center (Seoul, Republic of Korea). The protocols for the human urine assay were approved by the Ethics Committee of Asan Medical Center, and the methods for the human urine assay were carried out in accordance with the approved guidelines. The measurement was obtained by the same process as the standard curve measurement. The I_D–V_{BG} measurements were conducted at a drain voltage was of 4 V and a bottom gate sweep mode voltage ranging from −40 to +40 V.

Clinical Analysis: The preoperative PSA level in serum was measured using the immunoradiometric assay. The percent tumor volume was determined by the sum of all the visually estimated tumor foci of the prostate on each section.[34] The real tumor volume was calculated by multiplying with the percent tumor volume and the estimated prostate volume. The prostate tumor volume was estimated using the cross sectional and longitudinal images from MRI under the assumption that the prostate shape is an ellipsoidal solid.[35] The calculation method is Equations (1) and (2)

$$\text{Prostate volume} = \frac{\pi}{6} \times \text{transverse diameter} \times \text{AP diameter} \times \text{longitudinal diameter} \quad (1)$$

$$\text{Real tumor volume} = \%\,\text{tumor volume} \times \text{prostate volume} \quad (2)$$

Acknowledgements

M.J., S.P., and Y.K. contributed equally to this work. This research was supported by the Bio & Medical Technology Development Program of the NRF funded by the Korean government MSIP (2015M3A9E2029265) and KIST (KIST-AMC TRC program #2V05420).

Conflict of Interest

The authors declare no conflict of interest.

Keywords

annexin A3, noninvasive, prostate cancer, self-normalization, urine sensors

Received: April 6, 2017
Revised: May 22, 2017
Published online:

[1] J. Wilkosz, M. Brys, W. Rozanski, *Cent. Eur. J. Urol.* **2011**, *64*, 9.
[2] S. Jeong, J. Park, D. Pathania, C. M. Castro, R. Weissleder, H. Lee, *ACS Nano* **2016**, *10*, 1802.
[3] T. A. Douglas, D. Tamburro, C. Fredolini, B. H. Espina, B. S. Lepene, L. Ilag, V. Espina, E. F. Petricoin, L. A. Liotta, A. Luchini, *Biomaterials* **2011**, *32*, 1157.
[4] B. J. Kang, M. Jeun, G. H. Jang, S. H. Song, I. G. Jeong, C. S. Kim, P. C. Searson, K. H. Lee, *Int. J. Nanomed.* **2015**, *10*, 6555.
[5] R. L. Siegel, K. D. Miller, A. Jemal, *CA Cancer J. Clin.* **2015**, *65*, 5.
[6] D. Wirtz, K. Konstantopoulos, P. C. Searson, *Nat. Rev. Cancer* **2011**, *11*, 512.
[7] G. S. Gerber, G. W. Chodak, *Urol. Clin. North Am.* **1990**, *17*, 739.
[8] G. W. Chodak, P. Keller, H. W. Schoenberg, *J. Urol.* **1989**, *141*, 1136.
[9] E. D. Crawford, E. P. Deantoni, *Urol. Clin. North Am.* **1993**, *20*, 637.
[10] B. Xiang, D. W. Dong, N. Q. Shi, W. Gao, Z. Z. Yang, Y. Cui, D. Y. Cao, X. R. Qi, *Biomaterials* **2013**, *34*, 6976.
[11] W. J. Catalona, J. P. Richie, F. R. Ahmann, M. A. Hudson, P. T. Scardino, R. C. Flanigan, J. B. Dekernion, T. L. Ratliff, L. R. Kavoussi, B. L. Dalkin, W. B. Waters, M. T. Macfarlane, P. C. Southwick, *J. Urol.* **1994**, *151*, 1283.
[12] M. Schostak, G. P. Schwall, S. Poznanovic, K. Groebe, M. Muller, D. Messinger, K. Miller, H. Krause, A. Pelzer, W. Horninger, H. Klocker, J. Hennenlotter, S. Feyerabend, A. Stenzl, A. Schrattenholz, *J. Urol.* **2009**, *181*, 343.
[13] J. Kollerrmann, T. Schlomm, H. Bang, G. P. Schwall, C. von Eichel-Streibere, R. Simon, M. Schostak, H. Huland, W. Berg, G. Sauter, H. Klocker, A. Schrattenholz, *Eur. Urol.* **2008**, *54*, 1314.
[14] P. Beland, O. Krupin, P. Berini, *Biomed. Opt. Express* **2015**, *6*, 2908.
[15] M. P. van Gils, D. Hessels, O. van Hooj, S. A. Jannink, W. P. Peelen, S. L. Hanssen, J. A. Witjes, E. B. Cornel, H. F. Karthaus, G. A. Smits, G. A. Dijkman, P. F. Mulders, J. A. Schalken, *J. Urol.* **2007**, *177*, 568.
[16] W. H. Guan, X. X. Duan, M. A. Reed, *Biosens. Bioelectron.* **2014**, *51*, 225.
[17] H. C. Chen, Y. T. Chen, R. Y. Tsai, M. C. Chen, S. L. Chen, M. C. Xiao, C. L. Chen, M. Y. Hua, *Biosens. Bioelectron.* **2015**, *66*, 198.
[18] C. Hamelin-Peyron, V. Vlaeminck-Guillem, H. Haidous, G. P. Schwall, S. Poznanovic, E. Gorius-Gallet, S. Michel, A. Larue, M. Guillotte, A. Ruffion, G. Choquet-Kastylevsky, Y. Ataman-Onal, *Clin. Biochem.* **2014**, *47*, 901.
[19] I. K. Lee, M. Jeun, H. J. Jang, W. J. Cho, K. H. Lee, *Nanoscale* **2015**, *7*, 16789.
[20] T. A. Stamey, F. S. Freiha, J. E. Mcneal, E. A. Redwine, A. S. Whittemore, H. P. Schmid, *Cancer* **1993**, *71*, 933.
[21] D. Goncalves, D. M. F. Prazeres, V. Chu, J. P. Conde, *Biosens. Bioelectron.* **2008**, *24*, 545.
[22] H. J. Jang, J. Ahn, M. G. Kim, Y. B. Shin, M. Jeun, W. J. Cho, K. H. Lee, *Biosens. Bioelectron.* **2015**, *64*, 318.
[23] M. J. Spijkman, J. J. Brondijk, T. C. T. Geuns, E. C. P. Smits, T. Cramer, F. Zerbetto, P. Stoliar, F. Biscarini, P. W. M. Blom, D. M. de Leeuw, *Adv. Funct. Mater.* **2010**, *20*, 898.
[24] T. S. C. R. Rebelo, C. M. Pereira, M. G. F. Sales, J. P. Noronha, F. Silva, *Electrochim. Acta* **2016**, *190*, 887.
[25] Y. J. Kim, M. M. Rahman, J. J. Lee, *Sens. Actuators, B* **2013**, *177*, 172.
[26] G. Ploussard, J. I. Epstein, R. Montironi, P. R. Carroll, M. Wirth, M. O. Grimm, A. S. Bjartell, F. Montorsi, S. J. Freedland, A. Erbersdobler, T. H. van der Kwast, *Eur. Urol.* **2011**, *60*, 291.
[27] J. Noldus, T. A. Stamey, *J. Urol.* **1996**, *155*, 232.
[28] D. S. Park, J. Y. Hong, Y. K. Hong, S. R. Lee, J. H. Hwang, M. H. Kang, S. W. Kwon, J. J. Oh, *Urology* **2013**, *82*, 1394.
[29] C. Kim, J. F. Galloway, K. H. Lee, P. C. Searson, *Bioconjugate Chem.* **2014**, *25*, 1893.
[30] M. P. Hwang, J. W. Lee, K. E. Lee, K. H. Lee, *ACS Nano* **2013**, *7*, 8167.
[31] G. H. Jang, M. P. Hwang, S. Y. Kim, H. S. Jang, K. H. Lee, *Biomaterials* **2014**, *35*, 440.
[32] H. W. Son, M. Jeun, J. Choi, K. H. Lee, *Int. J. Nanomed.* **2017**, *12*, 2951.
[33] O. Zitka, N. Cernei, Z. Heger, M. Matousek, P. Kopel, J. Kynicky, M. Masarik, R. Kizek, V. Adam, *Electrophoresis* **2013**, *34*, 2639.
[34] C. Song, S. Seo, H. Ahn, S. S. Byun, J. S. Cho, Y. D. Choi, E. Lee, H. M. Lee, S. E. Lee, H. Y. Choi, *Int. J. Clin. Oncol.* **2012**, *17*, 355.
[35] S. H. Song, S. Pak, S. Park, C. Song, I. G. Jeong, H. J. Choi, J. K. Kim, K. S. Cho, C. S. Kim, H. Ahn, *J. Urol.* **2014**, *192*, 402.

